Vortex-induced vibrations of a flexible cylinder at large inclination angle

Rémi Bourguet, Michael S. Triantafyllou

Vortex-induced vibrations of a flexible cylinder at large inclination angle

Rémi Bourguet[1] and Michael S. Triantafyllou[2]

[1]Institut de Mécanique des Fluides de Toulouse, Université de Toulouse and CNRS, Toulouse, France

[2]Massachusetts Institute of Technology, Cambridge, MA, USA

The free vibrations of a flexible circular cylinder inclined at 80° within a uniform current are investigated by means of direct numerical simulation, at Reynolds number 500 based on the body diameter and inflow velocity. In spite of the large inclination angle, the cylinder exhibits regular in-line and cross-flow vibrations excited by the flow through the lock-in mechanism, i.e. synchronization of body motion and vortex formation. A profound reconfiguration of the wake is observed compared with the stationary body case. The vortex-induced vibrations are found to occur under parallel, but also oblique vortex shedding where the spanwise wavenumbers of the wake and structural response coincide. The shedding angle and frequency increase with the spanwise wavenumber. The cylinder vibrations and fluid forces present a persistent spanwise asymmetry which relates to the asymmetry of the local current relative to the body axis, owing to its in-line bending. In particular, the asymmetrical trend of flow–body energy transfer results in a monotonic orientation of the structural waves. Clockwise and counter-clockwise figure eight orbits of the body alternate along the span, but the latter are found to be more favourable to structure excitation. Additional simulations at normal incidence highlight a dramatic deviation from the independence principle, which states that the system behaviour is essentially driven by the normal component of the inflow velocity.

One contribution of 12 to a Theme Issue 'Advances in fluid mechanics for offshore engineering: a modelling perspective'.

Subject Areas:
ocean engineering, fluid mechanics

Keywords:
vortex-induced vibrations, inclined flexible cylinder, parallel and oblique vortex shedding, independence principle, direct numerical simulation

Author for correspondence:
Rémi Bourguet
e-mail: remi.bourguet@imft.fr

1. Introduction

Flow-induced vibrations (FIVs) of flexible bodies with bluff cross section are encountered in a great variety of physical systems, from the oscillations of plants in wind

to the vibrations of risers and mooring lines immersed in ocean currents. Such vibrations cause amplification of mean drag forces, increased fatigue damage and sometimes failure of the structures. Their prediction and the development of vibration reduction techniques require a detailed understanding of the underlying flow–structure interaction mechanisms. The impact of FIV in several civil, wind, offshore and nuclear engineering applications has motivated a number of studies, as collected in [1–3].

Vortex formation downstream of a bluff structure induces unsteady forces on the body which can lead to structural vibrations if the body is flexible. Vortex-induced vibrations (VIVs) of slender deformable structures placed in flow are a common type of FIV in ocean engineering. In practical applications, the flexible structures (e.g. marine risers, towing cables) are often inclined with respect to the direction of the oncoming current, sometimes at large angles. The VIVs that may appear in such configurations are the object of this work.

The canonical problem of a rigid cylinder forced or free to oscillate in the cross-flow direction within a current perpendicular to its axis has helped in clarifying in the fundamental phenomena of VIVs [4–13]. VIVs occur when the frequency of vortex formation and the frequency of body oscillation coincide; this condition of wake–body synchronization is referred to as lock-in. Under lock-in, the vortex shedding frequency can substantially depart from the Strouhal frequency, i.e. the shedding frequency downstream of a stationary body; also, the vibration frequency can shift considerably away from the structure natural frequency. The typical amplitude of VIV responses is of the order of one cylinder diameter in the cross-flow direction. When the rigid body is also allowed to oscillate in the in-line direction, vibrations of smaller amplitudes occur in this direction with a frequency ratio of 2 compared with the cross-flow response [14–16]. The VIVs of a long flexible cylinder placed in flow at normal incidence have also been well documented [17–22]. The lock-in mechanism results in oscillations of the slender deformable body with similar amplitudes to those noted in the rigid body case and a frequency ratio of 2 can generally be established between the in-line and cross-flow vibration components. However, the flexibility of the body and its distributed interaction with the flow may lead to an increased complexity of the responses, as, for instance, the occurrence of mixed standing–travelling structural waves or multi-frequency vibrations [23–27]. A notable feature related to the structure flexibility is the possible variability of the phase difference between the in-line and cross-flow vibrations along the cylinder; previous works have shown that the phase difference angle may drift along the span but remains locked to a specific range in the regions where the flow excites the flexible body [28,29].

Several studies concerning rigid cylinders, either fixed or forced to oscillate in the cross-flow direction, have emphasized that body inclination may have a considerable impact on flow patterns and fluid forcing [30–35]; yet vortex-induced excitation of the rigid body through lock-in still occurs in this context, even at inclination angles larger than 70° [36–40]. In the above-mentioned studies, the angle of inclination (α) is defined as the angle between the oncoming flow velocity direction and the plane perpendicular to the rigid cylinder axis, i.e. $\alpha = 0^\circ$ corresponds to the normal incidence configuration; this definition is adopted in this work based on the position of the flexible cylinder in quiescent fluid. Previous works have examined the possibility of likening the inclined body case to the normal incidence case. The independence principle (IP) or cosine law assumes that the flow dynamics is essentially determined by the component of the oncoming flow velocity perpendicular to the cylinder and that the component aligned with the cylinder axis, the axial component, has a negligible influence. According to the IP, the system behaviours in the inclined and normal configurations should thus match once the physical quantities (e.g. fluid forces, vortex shedding and body oscillation frequencies) are normalized by the inflow normal component; hence, the response of the system in the inclined case could be directly predicted based on the normal incidence case results. A remarkable effect of body inclination is the possible occurrence of oblique vortex shedding where the spanwise vortex rows forming downstream of the cylinder are not parallel to its axis. Oblique vortex shedding results in deviation from the IP [31]; the frequency of vortex formation under oblique shedding is usually larger than the frequency predicted by the IP [32,35]. In the fixed rigid cylinder case, the IP was shown to provide accurate predictions of the flow physics for $\alpha < 40^\circ$ approximately. A transverse oscillation of the

body tends to force parallel shedding [31,35,37]. This suggests an extended range of validity of the IP for a flexibly mounted rigid cylinder subjected to VIV; however, parallel shedding does not necessarily ensure validity of the IP [40].

In spite of its implications in engineering applications, the case of a slender flexible body inclined in flow has received much less attention. In a previous work [41], a flexible cylinder inclined at 60° within a uniform current was shown to exhibit VIV associated with parallel vortex shedding, whereas an oblique shedding pattern was observed in the stationary body case. The IP was found to provide an accurate prediction of the structural responses and fluid forces, as long as the in-line bending of the cylinder was small. A significant in-line bending induces a strong shear of the inflow velocity profile locally normal to the body, which may lead to multi-frequency vibrations and thus to a deviation from the IP; even in this case, the predominant vibration frequency was found to be in agreement with the IP.

When the flexible cylinder is placed at a larger inclination angle, the behaviour of the flow–structure system remains to be investigated. The occurrence of VIV and the possible application of the IP in this case still need to be elucidated. Previous studies concerning rigid cylinders indicate that the fluid loading caused by the slanted vortex formation in the case of oblique shedding would not lead to excitation of the body, owing to the alternating sign of the fluctuating forces along the span [35,42]. For a flexible body at a large inclination angle, the question arises whether such oblique shedding may induce vibrations (i.e. far from IP validity conditions), and, if the lock-in condition is established, what will be the reciprocal influence of the flexible structure oscillations on the slanted shedding pattern. To address these aspects, a combined wake–body analysis is presented on the basis of high-resolution simulation results issued from direct numerical simulations of the flow past a flexible circular cylinder of length to diameter aspect ratio 50, placed at 80° of inclination in a uniform current at Reynolds number 500, based on the inflow velocity and cylinder diameter. The flexible cylinder is modelled as a tension-dominated structure, and different values of the tension are selected in order to explore a range of typical responses of the system.

The paper is organized as follows. The fluid–structure model and the numerical method are described in §2. The fixed rigid cylinder case, which represents a baseline configuration to quantify the modifications associated with body oscillations in the following, is briefly considered in §3. The flexible cylinder case is examined in §4. The main findings of the present study are summarized in §5.

2. Formulation and numerical method

The physical configuration is similar to that considered in a previous work concerning the VIV of a flexible cylinder at lower inclination angle [41]. The cylinder has a circular cross section and a length (L) to diameter (D) aspect ratio $L/D = 50$; it is pinned at both ends and free to oscillate in the in-line (x-axis) and cross-flow (y-axis) directions. The cylinder is inclined at $\alpha = 80^\circ$ within a uniform flow of velocity magnitude U. The Reynolds number based on U and D, $Re = \rho_f UD/\mu$, where ρ_f and μ denote the fluid density and viscosity, is set equal to 500. Similar to the inclination angle α, the axial and normal components of the oncoming flow are defined based on the position of the cylinder in quiescent fluid. The inflow axial component refers to the component parallel to the cylinder in a fluid at rest (z-axis), and the inflow normal component designates the component aligned with the x-axis. The velocity magnitude of the inflow normal component is $U_n = U\cos(\alpha)$ and the associated Reynolds number $Re_n = Re\cos(\alpha) = 86.8$. The physical quantities normalized by U_n are denoted by the subscript $(\,)_n$ in the following. For comparison purposes, a normal incidence configuration where the inflow axial component is removed is also considered. Previous works, for example [34], suggested that application of the IP should also include an appropriate scaling of the Reynolds number, i.e. the Reynolds number selected in the normal incidence case should match the Reynolds number based on U_n in the inclined body case, instead of U. In order to assess the validity of the IP, both values of the Reynolds number ($Re_n = 500$ and $Re_n = 86.8$) are considered in the present normal incidence configuration.

The physical variables are non-dimensionalized by ρ_f, D and U. The cylinder mass ratio, defined as $m = \rho_c/\rho_f D^2$, where ρ_c is the cylinder mass per unit length, is set to 6. The constant tension and damping of the structure are designated by τ and η. The non-dimensional tension is defined as $T = \tau/\rho_f D^2 U^2$ and the non-dimensional damping as $K = \eta/\rho_f DU$. The non-dimensional displacements of the cylinder in the in-line and cross-flow directions are denoted by ζ_x and ζ_y. The sectional in-line and cross-flow force coefficients are defined as $C_x = 2F_x/\rho_f DU^2$ and $C_y = 2F_y/\rho_f DU^2$, where F_x and F_y are the in-line and cross-flow dimensional sectional fluid forces. The structural dynamics are governed by forced vibrating string equations which can be expressed as follows [23]:

$$m\ddot{\zeta}_{\{x,y\}} - T\zeta''_{\{x,y\}} + K\dot{\zeta}_{\{x,y\}} = \frac{C_{\{x,y\}}}{2}, \tag{2.1}$$

where $\dot{}$ and $'$ denote the time and space derivatives. The string non-dimensional phase velocity is $\omega = \sqrt{T/m}$. In order to cover a range of structural responses, three values of T, 54, 37.5 and 13.5, are selected. The structural damping is set equal to zero ($K = 0$) to allow maximum amplitude oscillations. As a preliminary step of the study, the case of a fixed rigid cylinder aligned with the z-axis ($\zeta_{\{x,y\}} = 0$) is also considered.

The flow past the cylinder is predicted using direct numerical simulation of the three-dimensional incompressible Navier–Stokes equations. The parallelized code *Nektar*, based on the spectral/*hp* element method [43], is used to solve the coupled flow–structure system. The version of the code employs a Jacobi–Galerkin formulation in the (x, y) plane and a Fourier expansion in the spanwise (z) direction. A boundary-fitted coordinate formulation is used to take into account the cylinder unsteady deformation. Details concerning the numerical method and its validation have been reported in [44,45] for similar configurations. The computational domain ($50D$ downstream and $20D$ in front, above, and below the cylinder), boundary conditions (no-slip condition on the cylinder surface, flow periodicity on the side boundaries) and discretization (2175 elements with polynomial order $p = 7$ in the (x, y) plane and 512 complex Fourier modes in the z-direction) are the same as in [22,41]. The present analysis is based on time series of more than 800 time units. Convergence of each simulation is established by monitoring the mean and root mean square (RMS) values of the fluid force coefficients and body displacements.

3. Fixed rigid cylinder

Before investigating the behaviour of the coupled flow–structure system, the case of a fixed rigid cylinder is briefly considered in this section. The objective is to characterize the main features of the flow and of the fluid forces in the absence of body motion, and to assess the validity of the IP in this context.

An overview of the flow past the inclined stationary cylinder is presented in figure 1*a* by means of instantaneous isosurfaces of the spanwise vorticity (z component); the vorticity is non-dimensionalized using U_n. For comparison purpose, the flow past the fixed rigid cylinder at normal incidence ($Re_n = 500$) is visualized in figure 1*b*. As also reported in previous studies concerning rigid cylinders at similar inclination angles [35,37], the wake of the inclined stationary body is composed of obliquely shed vortex rows, contrary to the normal incidence case where the vortex rows are parallel to the cylinder axis. The vortices are peeling off from the cylinder with an angle approximately equal to 16° with respect to the cylinder axis; their inclination increases in the near region and the angle of the straight slanted vortex rows observed in the wake is equal to 66° approximately, i.e. relatively close but not equal to the body inclination angle. In spite of its oblique orientation, the wake structure resembles the 2S pattern [6] occurring at normal incidence: at each spanwise location, two counter-rotating vortices form per shedding period. The frequency of vortex shedding, established from the time series of the cross-flow component of the flow velocity $10D$ downstream of the cylinder, and non-dimensionalized using U_n is reported in table 1 (f_{vn}) for the inclined body and the normal incidence configurations. As previously mentioned, two values of the Reynolds number are considered at normal incidence: $Re_n = 500$ and $Re_n = 86.8$, which correspond to the values of Re and Re_n in the inclined body case. Regardless

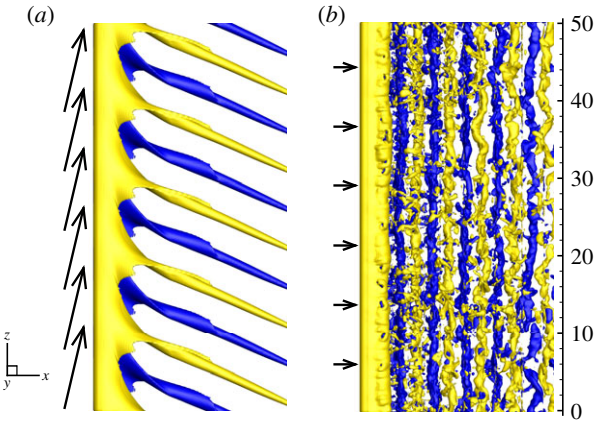

Figure 1. Instantaneous isosurfaces of the spanwise vorticity in the (*a*) inclined ($Re = 500$, $\omega_{zn} = \pm 0.48$) and (*b*) normal ($Re_n = 500$, $\omega_{zn} = \pm 1.73$) fixed rigid cylinder configurations. Arrows represent the oncoming flow. Part of the computational domain is shown. (Online version in colour.)

Table 1. Vortex shedding frequency and span-averaged values of the mean in-line force coefficient, RMS in-line force coefficient fluctuation and RMS cross-flow force coefficient, in the inclined and normal fixed rigid cylinder configurations.

	f_{vn}	$\langle \bar{C}_{xn} \rangle$	$\langle (\tilde{C}_{xn})_{\mathrm{RMS}} \rangle$	$\langle (C_{yn})_{\mathrm{RMS}} \rangle$
inclined cylinder, $Re = 500$, $Re_n = 86.8$	0.593	1.618	0.031	0.675
normal cylinder, $Re_n = 500$	0.208	1.141	0.043	0.250
normal cylinder, $Re_n = 86.8$	0.159	1.362	0.004	0.194

of the Reynolds number value selected in the normal incidence configuration, the frequency of vortex formation is substantially larger for the oblique shedding pattern observed downstream of the inclined cylinder.

The fluid forces exhibit temporal fluctuations at each spanwise location, but the alternation of positive and negative oblique vortices forming continuously along the inclined cylinder results in constant values of the span-averaged forces ($\langle C_x \rangle = \langle \bar{C}_x \rangle$ and $\langle C_y \rangle = 0$, where $\bar{}$ and $\langle\ \rangle$ denote the time- and span-averaging operators), as also mentioned by Mittal & Sidharth [42]. The absence of temporal fluctuations of the span-averaged forces suggests that the slanted shedding pattern would not excite the rigid cylinder if it was free to oscillate. However, vortex-induced excitation remains possible for a flexible structure; this aspect will be studied in §4. The span-averaged values of the mean in-line force coefficient, RMS in-line force coefficient fluctuation and RMS cross-flow force coefficient exerted on the stationary cylinder are presented in table 1; in table 1 and in the following, the fluctuations are denoted by $\tilde{}$. The fluid forces are non-dimensionalized by U_n. Clear differences can be noted between the inclined and normal body configurations. In particular, the mean in-line force is significantly larger in the inclined cylinder case.

The physical quantities in the inclined and normal body cases do not match after normalization by U_n; therefore, the IP is not valid for the stationary cylinder, in agreement with previous works. It can be noted that the shedding frequency and fluid forces in the inclined and normal configurations differ even if the magnitude of the inflow velocity component normal to the vortex rows is used in the normalization.

The case of the fixed rigid cylinder at 80° is thus characterized by a strongly inclined vortex shedding pattern and a clear departure from the IP. The flexible body configuration is addressed in the following.

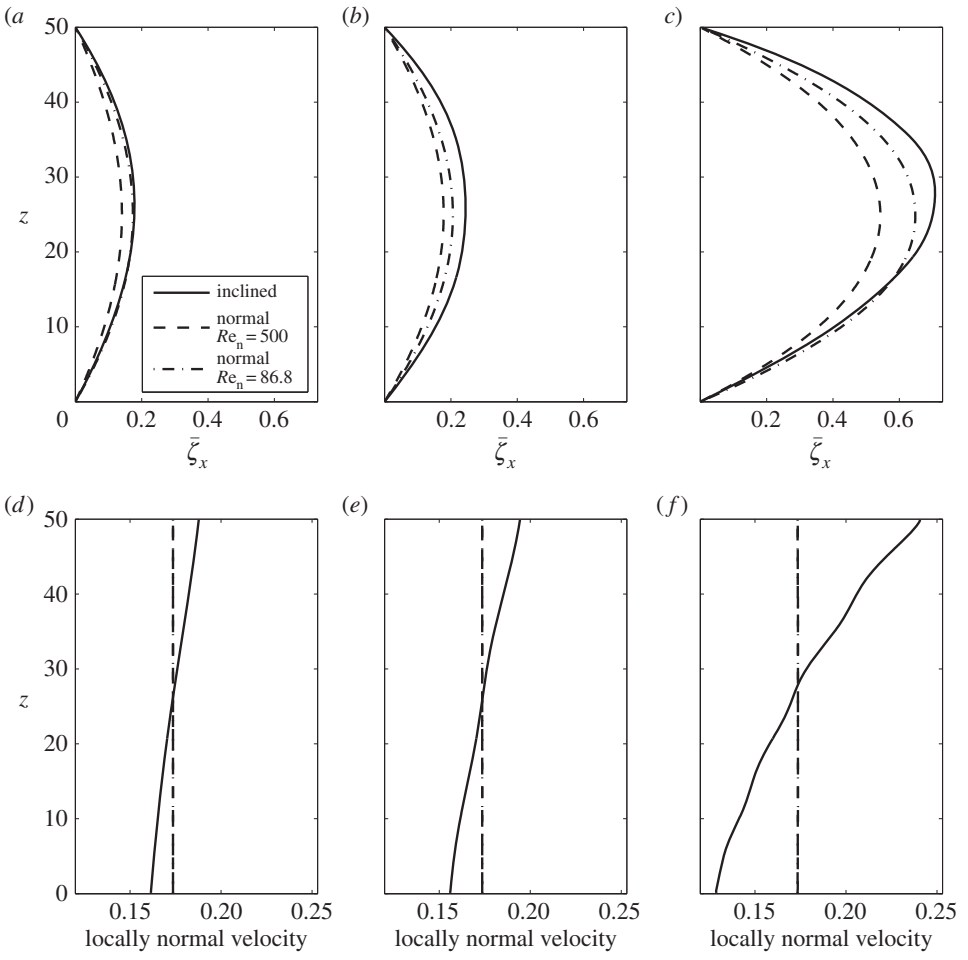

Figure 2. (*a–c*) Mean in-line displacement of the cylinder and (*d–f*) inflow velocity component locally normal to the cylinder, along the span, for (*a*,*d*) $T = 54$, (*b*,*e*) $T = 37.5$ and (*c*,*f*) $T = 13.5$.

4. Flexible cylinder

The behaviour of the flow–structure system and the validity of the IP are investigated in this section for three values of the flexible cylinder tension. The flexible body responses are quantified in §4*a*. The flow patterns and the occurrence of wake–body synchronization are examined in §4*b*. The fluid forces and flow–structure energy transfer are analysed in §4*c*.

(a) Structural responses

The mean in-line displacement of the inclined cylinder along its span is plotted in figure 2*a–c* for each value of the tension. The in-line bending of the cylinder increases as T decreases, but remains lower than 1.5% of the body length. The in-line curvature induces an asymmetry of the inflow velocity profiles locally normal and parallel to the inclined cylinder along its span; an asymmetry may thus be expected in the flow–structure system behaviour. In particular, owing to the large angle of inclination, a small in-line bending results in a significant shear of the current velocity locally normal to the body; its magnitude, which increases with z, is equal to $U\cos(\alpha + \theta)$, where θ is the local angle between the z-axis and the cylinder axis in its mean position. The magnitude of the locally normal velocity, non-dimensionalized by U, is presented in figure 2*d–f*; it ranges from 0.16 ($z = 0$) to 0.19 ($z = 50$), for $T = 54$, and from 0.13 ($z = 0$) to 0.24 ($z = 50$), for $T = 13.5$. It can

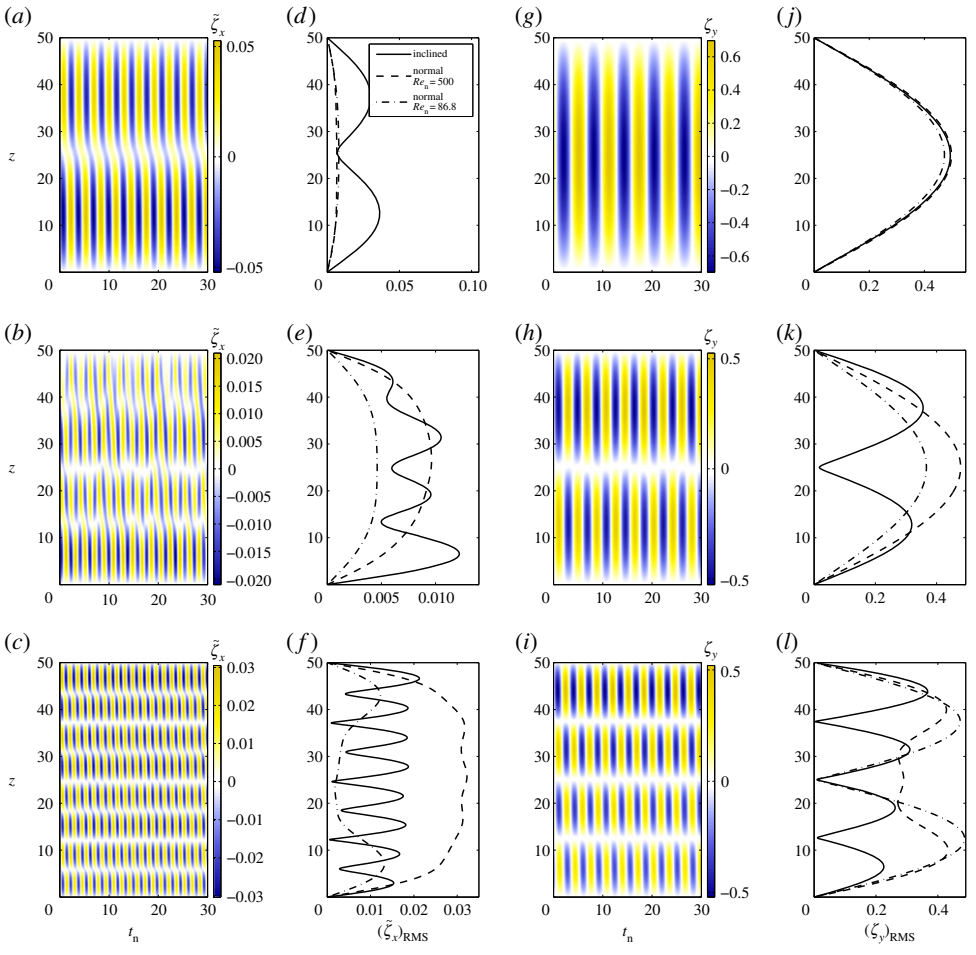

Figure 3. (*a–c*) Selected time series of the inclined cylinder in-line displacement fluctuation, (*d–f*) RMS in-line displacement fluctuation, (*g–i*) selected time series of the inclined cylinder cross-flow displacement and (*j–l*) RMS cross-flow displacement, along the span, for (*a,d,g,j*) $T = 54$, (*b,e,h,k*) $T = 37.5$ and (*c,f,i,l*) $T = 13.5$. (Online version in colour.)

be observed that the point of maximum mean displacement tends to shift towards $z = 50$, i.e. the region of large magnitude of the locally normal current.

As in the fixed rigid cylinder case, the normal incidence results for $Re_n = 500$ and $Re_n = 86.8$ are also reported in order to quantify the impact of the inflow axial component and assess the IP validity. In general, it can be noted that the amplitude of the in-line bending differs between the inclined and normal cylinder cases (figure 2*a–c*). The body curvature remains symmetrical about the mid-span point in the latter case. Contrary to the inclined body configuration, the profile of the inflow velocity locally perpendicular to the cylinder at normal incidence ($U_n \cos(\theta)$) is very close to uniform, as shown in figure 2*d–f*.

Selected time series of the in-line and cross-flow displacements of the inclined cylinder and associated RMS values are plotted along the span in figure 3. In these plots, the fluctuation of the in-line displacement about the body mean position is considered, and the non-dimensional time variable t is normalized using U_n (t_n). In all studied cases, the inclined cylinder exhibits regular oscillations in both directions. The structural responses consist of mixed standing–travelling wave vibrations with a predominant standing wave nature. The vibration amplitudes are comparable to those reported in previous studies concerning flexible cylinders at normal incidence [17,20,22] or lower inclination angle [41] and the smaller amplitudes of the in-line responses, compared

Table 2. Cross-flow vibration frequency, spatial wavenumber, structural mode and natural frequency associated with the excited wavenumber in the inclined cylinder configuration and cross-flow vibration frequency in the normal cylinder configuration, as functions of the tension/phase velocity.

		inclined cylinder				normal cylinder	
		$Re = 500$, $Re_n = 86.8$				$Re_n = 500$	$Re_n = 86.8$
T	ω	f_{yn}	k_y	n_y	$f_{nat_n}(k_y)$	f_{yn}	f_{yn}
54	3	0.165	0.01	1	0.162	0.171	0.168
37.5	2.5	0.262	0.02	2	0.271	0.143	0.143
13.5	1.5	0.318	0.04	4	0.325	0.167	0.167

with the cross-flow oscillations, were also noted in these works. The vibrations generally present a spanwise asymmetry, as expected owing to the asymmetry of the local inflow velocity profiles induced by the in-line bending. The inclined body responses are dominated by a single frequency and a single structural wavenumber in each direction. A ratio of 2 can be established between the in-line and cross-flow vibration frequencies, as also observed in the above mentioned studies. The excited structural wavenumbers increase as T decreases. In all cases, the in-line and cross-flow vibration wavenumbers exhibit a ratio of 2; the linear dispersion relation of a string in vacuum and the frequency ratio of 2 suggest such ratio between the excited wavenumbers. The principal characteristics of the structural response are presented in table 2; because of the above-mentioned ratio between the in-line and cross-flow frequencies/wavenumbers, only the cross-flow response properties are reported. The vibration frequency is non-dimensionalized by U_n (f_{yn}). The sine Fourier mode number n_y (nth mode defined as $\sin(\pi nzD/L)$) associated with the excited wavenumber k_y ($n_y = 2k_yL/D$) is also reported. The following dispersion relation is used to estimate the natural frequency f_{nat} associated with the structural wavenumber k when the body is immersed in fluid:

$$f_{nat}(k) = k\omega\sqrt{\frac{m}{m + (\pi/4)C_m}}, \tag{4.1}$$

where C_m is the added mass coefficient induced by the fluid forces in phase with the cylinder acceleration. The natural frequencies normalized by U_n (f_{nat_n}), and associated with the excited wavenumbers, for $C_m = 1$, are indicated in table 2. The actual vibration frequencies remain close to the natural frequencies predicted by the above dispersion relation.

The RMS values of the displacement amplitudes and the cross-flow vibration frequencies in the normal incidence configuration are also presented in figure 3 and table 2, for $Re_n = 500$ and $Re_n = 86.8$. Although the responses of the inclined and normal cylinders appear relatively close in some specific cases, e.g. cross-flow displacement at $T = 54$ (figure 3*j*), it can be observed that they do not match in general. The normal cylinder responses remain essentially symmetrical, which is not the case for the inclined body. As a consequence, at the present large inclination angle, the IP which was found to fail for a stationary cylinder, also fails when the cylinder is subjected to free vibrations. In a previous work concerning a flexible cylinder at lower inclination angle ($\alpha = 60°$) [41], the deviation from the IP was attributed to the in-line bending of the structure; among others, the IP does not take into account the shear of the current locally perpendicular to the body owing to its curvature. In that previous study, it was shown that introducing, in the normal incidence case, a sheared velocity profile matching the locally perpendicular inflow component, leads to responses comparable to those occurring in the inclined body configuration. Additional simulations with modified inflow profiles indicate that this result cannot be extended to the present inclination angle: even if the locally perpendicular velocity profile is the same, the responses of the inclined and normal cylinders still differ. This shows that the system behaviour is

not only driven by the locally normal inflow component and that the locally parallel component may also become a crucial element at large inclination angle.

The cross-flow vibration frequency of the inclined cylinder is close to the normal case oscillation frequency for $T = 54$, but clearly deviates when the tension is reduced. Such deviation of the vibration frequency was not observed at lower inclination angle [41]. The inclined body vibration frequency increases as T decreases and it reaches high values compared with the typical frequencies reported in the literature on flexible cylinder VIV [17,18,44]. The broad range of response frequencies raises the question of the nature of the interaction between the flexible structure and the flow, and more precisely, the possible occurrence of wake–body synchronization in this context. This question is clarified in §4*b*.

For a better analysis of the mixed standing–travelling wave nature of the inclined cylinder responses, the displacements can be approximated as follows, using $N+1$ temporal Fourier modes:

$$\zeta_{\{x,y\}}(z,t) \approx \sum_{s=-N/2}^{N/2} a^{\mathrm{s}}_{\{x,y\}}(z)\exp(2\pi \mathrm{i} f^{\mathrm{s}} t) = \sum_{s=-N/2}^{N/2} |a^{\mathrm{s}}_{\{x,y\}}|(z)\exp(\mathrm{i}(2\pi f^{\mathrm{s}} t + \Psi^{\mathrm{s}}_{\{x,y\}}(z))), \tag{4.2}$$

where $f^{\mathrm{s}} = s/\mathcal{T}$ and $\mathcal{T}$ is the sampling period. The complex modal coefficients a^{s}_x and a^{s}_y are written in terms of their moduli and their spatial phases Ψ^{s}_x and Ψ^{s}_y. The spanwise evolutions of the unwrapped spatial phases associated with the in-line and cross-flow vibration frequencies (for $s > 0$) are plotted in figure 4*a–c*, for each value of the tension. The strong standing wave nature of the responses is confirmed by the zigzagging trends of the phases. It can also be noted that for all cases, the value of the phase tends to increase with z along the span. Therefore, the structural vibrations of the inclined cylinder present a slight travelling wave behaviour orientated from $z = 50$ to $z = 0$ (decreasing z). The structural waves thus follow the shear of the inflow velocity component locally normal to the cylinder, i.e. they travel from the region of large normal flow velocity to the region of low normal velocity. The preferential orientation of the waves will be connected to the fluid forcing in §4*c*. Such systematic orientation of the structural waves is not observed at normal incidence.

The frequency ratio of 2 identified between the in-line and cross-flow vibrations results in figure eight trajectories of the cylinder in the plane perpendicular to the span, as illustrated in figure 4*d–i*. The phase difference between the in-line and cross-flow vibration components occurring at frequencies $2f^{\mathrm{s}}$ and f^{s}, respectively, is evaluated as follows:

$$\Phi^{\mathrm{s}}_{xy} = \Psi^{2s}_x - 2\Psi^{\mathrm{s}}_y. \tag{4.3}$$

In the present case where a single frequency is excited in each direction, the shape and orientation of the cylinder trajectory are determined, at each spanwise location, by a single phase difference Φ^{s}_{xy}. Values of this phase difference in the range 0–180° (180–360°, respectively) correspond to figure eight orbits where the body moves upstream (downstream, respectively) when reaching the cross-flow oscillation maxima; these two types of trajectories are referred to as counter-clockwise and clockwise, respectively [46]. The spanwise evolution of the phase difference in the inclined body case is plotted in figure 4*j–l* for each value of the tension; the locations of the points selected in figure 4*d–i* are indicated by dashed lines and the limit between counter-clockwise and clockwise orbits (180°) is denoted by a plain line. The spanwise patterns of the in-line/cross-flow response synchronization differ in the normal incidence cases, as expected owing to the differences pointed out previously in the structural vibrations; they are not presented here. As detailed in a prior work concerning flexible cylinders at normal incidence [29], the strong standing wave nature of the inclined cylinder vibrations results in a well-defined alternation of counter-clockwise and clockwise orbits along the span; the transition between the two types of orbits occurs near the minima of the in-line response amplitude. Previous studies have emphasized that the orientation of the trajectory is closely related to the transfer of energy between the flow and the flexible body [28,29]; this aspect, which remains to be investigated in the inclined cylinder case, will be addressed in §4*c*.

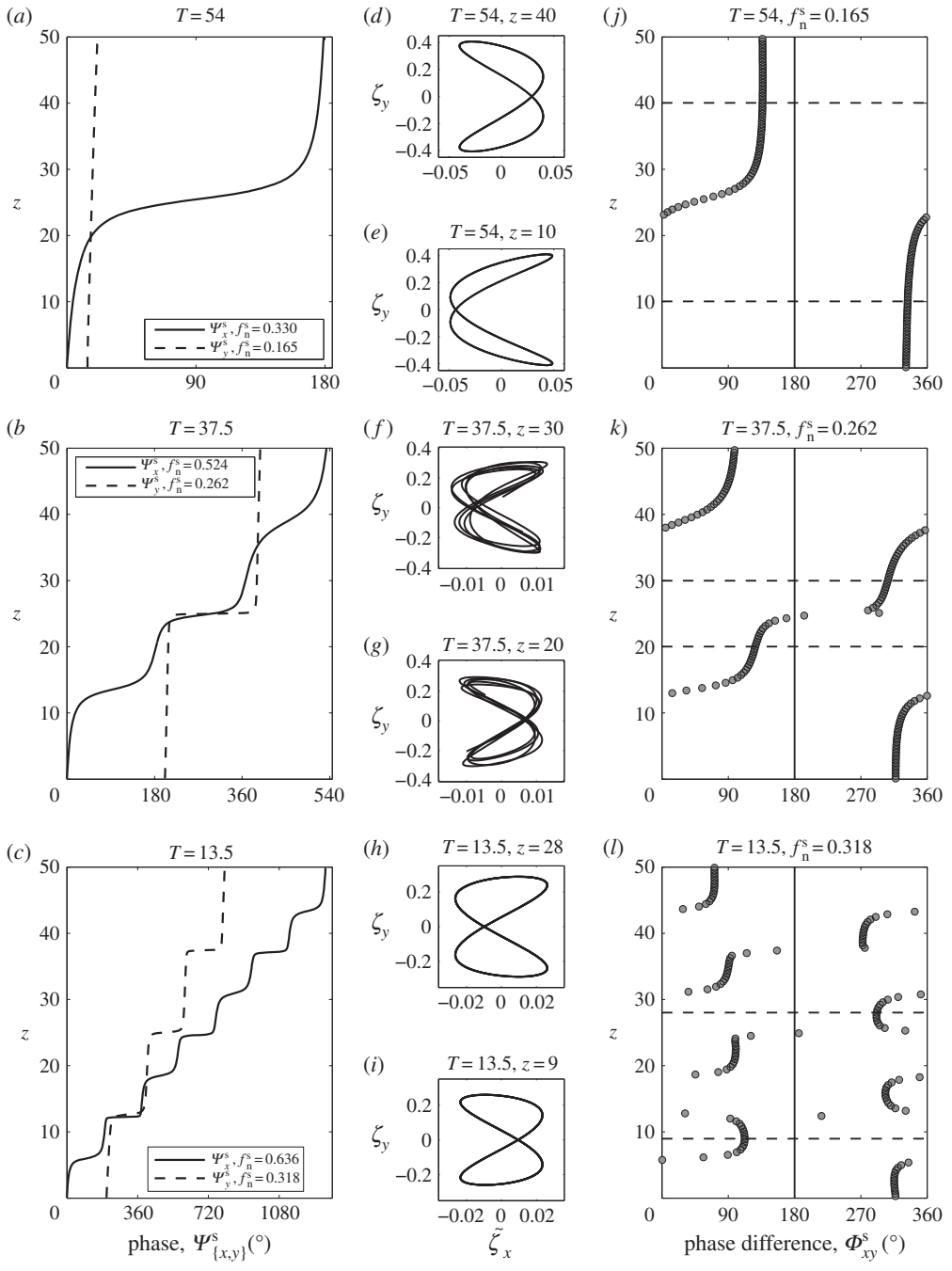

Figure 4. (*a–c*) Unwrapped spatial phases of the in-line and cross-flow displacements along the span. (*d–i*) Typical trajectories at selected spanwise locations. (*j–l*) Spanwise evolution of the phase difference between the in-line and cross-flow displacements. The reported results concern the inclined cylinder configuration for (*a,d,e,j*) $T = 54$, (*b,f,g,k*) $T = 37.5$ and (*c,h,i,l*) $T = 13.5$. The locations of the monitoring points in (*d–i*) are indicated by dashed lines in (*j–l*), and the limit between counter-clockwise and clockwise trajectories (180°) is denoted by a plain line.

The above analysis shows that the flexible cylinder inclined at 80° is subjected to regular free oscillations but that the IP is not valid for the prediction of the structural responses. In §4*b*, the inclined body vibrations are connected to the flow patterns occurring in its wake.

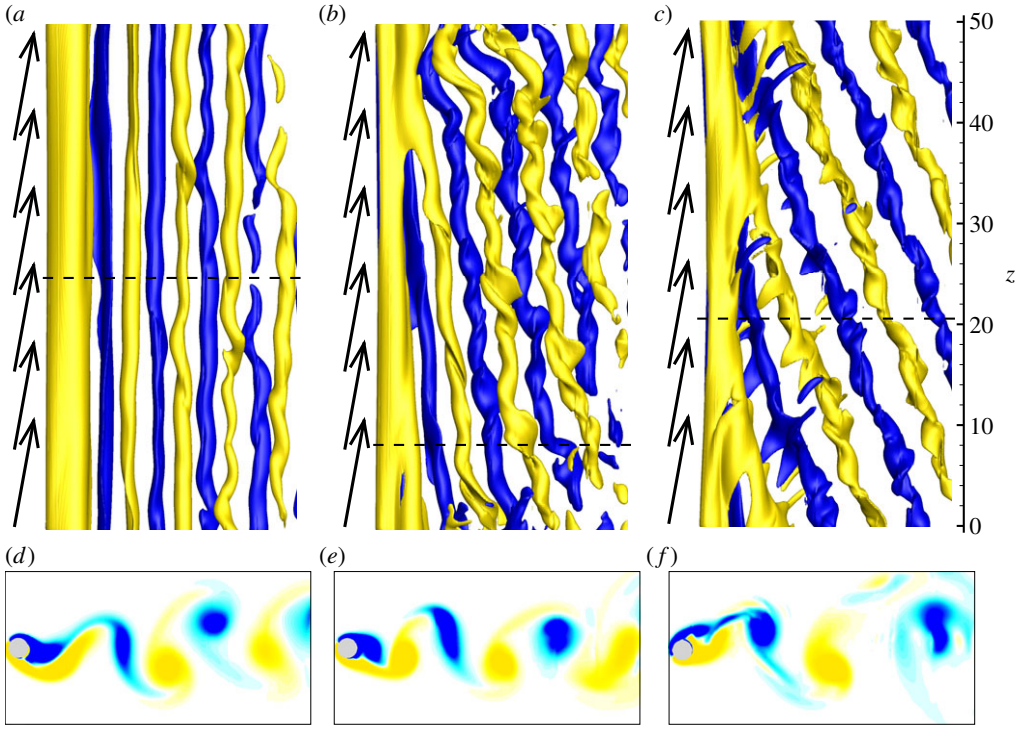

Figure 5. (*a–c*) Instantaneous isosurfaces ($\omega_{zn} = \pm 0.58$) and (*d–f*) isocontours in the (x, y) plane ($\omega_{zn} \in [-1.04, 1.04]$) of the spanwise vorticity in the inclined cylinder configuration, for (*a*,*d*) $T = 54$, (*b*,*e*) $T = 37.5$ and (*c*,*f*) $T = 13.5$. In (*a–c*), arrows represent the oncoming flow and the spanwise locations selected in (*d–f*) are indicated by dashed lines. Part of the computational domain is shown. (Online version in colour.)

(b) Flow patterns and wake–body synchronization

The flow past the freely vibrating inclined cylinder is visualized in figure 5*a–c* through instantaneous isosurfaces of the spanwise vorticity, for the three values of the tension. A striking feature is that each case exhibits a different angle of inclination of the vortex rows occurring in the wake. For $T = 54$, the vortices are found to be essentially parallel to the cylinder, as in the normal incidence configuration where parallel shedding is noted for all simulated cases. Such transition from oblique to parallel shedding once the body oscillates was also reported in previous studies for a flexible cylinder at 60° [41] and a rigid cylinder up to 70° [37,40]; the present results indicate that this phenomenon persists in the case of a flexible cylinder inclined at 80°. In contrast, oblique shedding is observed for the lower values of the tension; the angle between the vortex rows and the z-axis is approximately equal to 7° for $T = 37.5$ and 20° for $T = 13.5$, versus 66° in the stationary body case. The vortices present slightly lower slant angles as they are peeling off from the cylinder, and a small bending of the vortex rows can be noted in the near wake region, as also observed in the fixed rigid cylinder case (§3); the above-mentioned values correspond to the inclination angles of the developed straight vortex rows. Instantaneous isocontours of the spanwise vorticity in the (x,y) plane, at selected locations indicated by dashed lines in figure 5*a–c*, are presented in figure 5*d–f*. As in the fixed rigid cylinder case, the wake is characterized by the formation of two counter-rotating vortices per shedding cycle, i.e. the 2S pattern.

In order to quantify the spatio-temporal properties of the wake and connect them to the structural responses, a detailed analysis of the cross-flow component of the flow velocity (v), along a line parallel to the z-axis and located $10D$ downstream of the cylinder, is reported in the following. Selected time series of v are plotted in figure 6*a–c*, for the three values of the tension. The parallel or oblique nature of the wake pattern as a function of T can be clearly

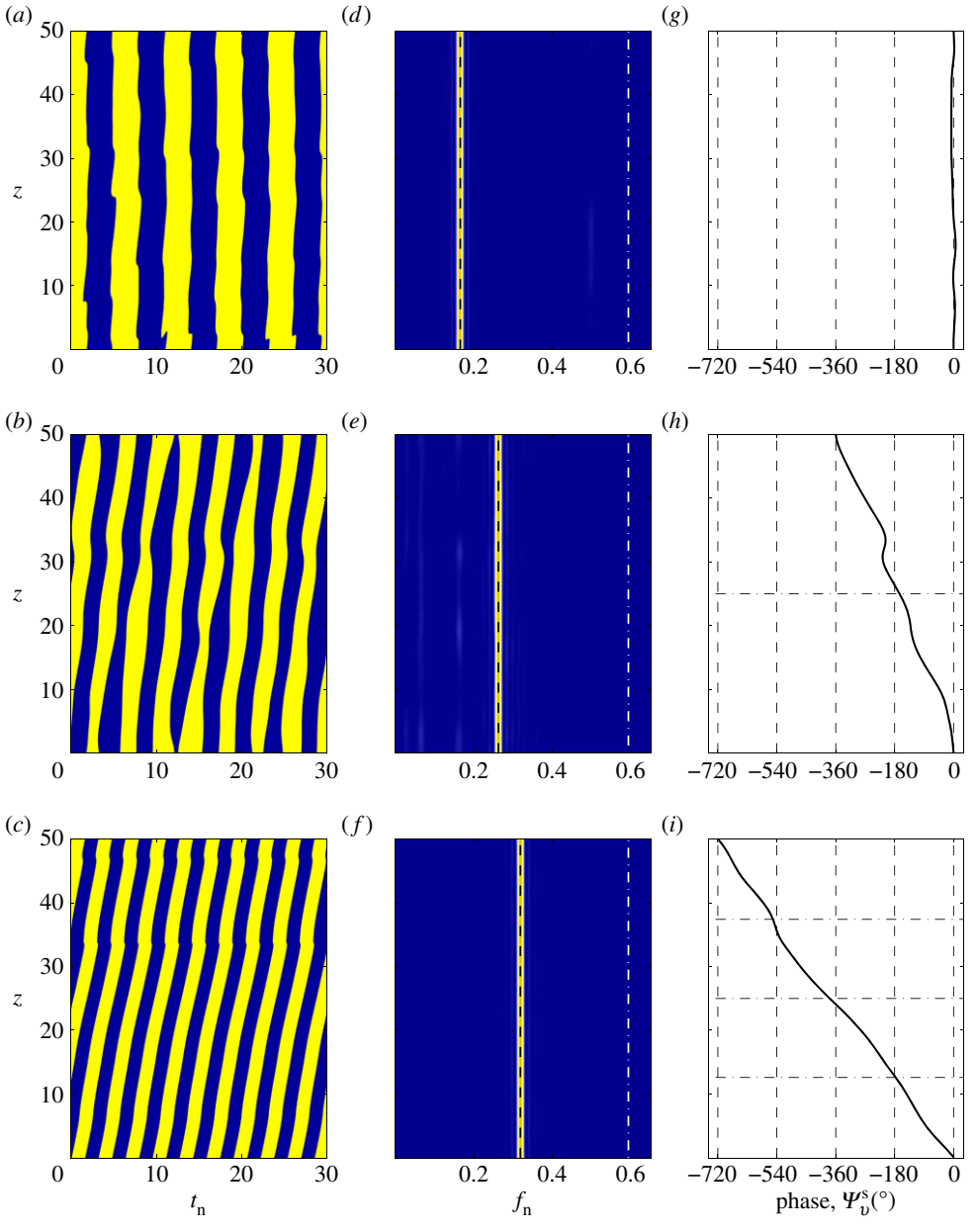

Figure 6. (*a–c*) Selected time series of the cross-flow component of flow velocity 10*D* downstream of the inclined cylinder (positive/negative values in yellow/blue) and associated (*d–f*) PSD and (*g–i*) unwrapped spatial phase, along the span, for (*a*,*d*,*g*) $T = 54$, (*b*,*e*,*h*) $T = 37.5$ and (*c*,*f*,*i*) $T = 13.5$. In (*d–f*), the PSD is normalized by the magnitude of the largest peak at each spanwise location and the colour bar levels range from 0 (blue) to 1 (yellow); the cross-flow vibration frequency is indicated by a black dashed line and the vortex shedding frequency observed in the absence of structural oscillation by a white dashed-dotted line. In (*h*,*i*), dashed-dotted lines denote the minima of the cross-flow vibration envelope. (Online version in colour.)

identified in these plots. The power spectral density (PSD) of v, presented in figure 6*d–f*, is used to determine the vortex shedding frequency at each point of the body length. In these plots, the PSD is normalized by its largest magnitude and the frequency is non-dimensionalized by U_n (f_n). For each value of the tension, the vortex shedding frequency is constant along the span and matches the cross-flow vibration frequency (indicated by a black dashed line). Therefore,

the lock-in condition is established along the entire cylinder length, as also observed at normal incidence. To the best of the authors' knowledge, the appearance of the lock-in condition for a flexible cylinder at such large inclination angle was not previously reported. In all studied cases, independently of the slant angle of the vortex rows, the excitation of the inclined flexible cylinder by the flow thus occurs through synchronization between the body oscillation and the vortex formation; that is why the responses of the inclined cylinder are referred to as VIV.

The vortex shedding frequency downstream of the vibrating cylinder is considerably reduced compared with the frequency observed in the absence of structural oscillation, which is denoted by a white dashed-dotted line in figure 6*d–f*. Because the lock-in condition is established in all cases, the vibration frequencies reported in table 2 correspond to the vortex shedding frequencies. When the vortex rows are parallel to the inclined body ($T = 54$), the shedding frequency remains close to the frequency identified at normal incidence; yet this does not imply validity of the IP, as shown in §4*a* (e.g. figure 3*d*). As also noted by earlier studies [35,37] for fixed rigid cylinders inclined in flow, the vortices exhibit larger formation frequency under oblique shedding than under parallel shedding. In the oblique pattern case, the IP substantially underestimates the shedding (and vibration) frequency.

For flexible cylinders subjected to VIV under parallel shedding, previous works have shown that the alternating regions of positive and negative transverse displacement along the span are associated with the simultaneous formation of vortex rows of opposite vorticity signs along the cylinder length [41,44]; this observation suggests a coincidence between the spanwise wavenumber of the wake pattern and the excited structural wavenumber. To clarify this aspect in the present configuration, the cross-flow velocity component v is approximated by a Fourier expansion similar to (4.2) and the unwrapped spatial phase Ψ_v^s associated with the predominant frequency of v (for $s > 0$) is plotted along the span in figure 6*g–i*, for each value of the tension. For $T = 54$, under parallel shedding, the phase remains relatively constant along the cylinder length. In contrast, the phase regularly decreases along the span for $T = 37.5$ and $T = 13.5$, in agreement with the inclination of the wake. The locations of the minima of the cross-flow vibration are indicated by dashed-dotted lines in figure 6*h,i*; they essentially correspond to the nodes of the associated sine Fourier mode (n_y) and the distance between two successive minima is equal to $1/2k_y$. It appears that the phase of v exhibits variations of approximately -180° between each minimum of the cross-flow vibration. The spanwise wavenumber of the oblique wake pattern thus matches the excited structural wavenumber (0.02 for $T = 37.5$ and 0.04 for $T = 13.5$); hence, the cylinder vibration and the wake pattern are found to be spatially locked. As also observed in the absence of vibration in [35], the slant angle and shedding frequency tend to increase with the spanwise wavenumber, which increases when the tension is reduced in the flexible body case.

The present observations show that the vibrations of the inclined flexible cylinder occur under the lock-in condition and that this state of wake–body synchronization is accompanied by a profound reconfiguration of the flow pattern compared with the fixed rigid cylinder case, both temporally, with a substantial alteration of the vortex formation frequency, and spatially, with a modification of the shedding angle. The forcing exerted by the flow on the vibrating inclined body is examined in the following.

(c) Fluid forces and flow–structure energy transfer

The spanwise evolutions of the mean in-line force coefficient and of the RMS in-line and cross-flow force coefficients are plotted in figure 7*a–i*, for the three values of the tension; in figure 7*d–f*, the fluctuation of the in-line force coefficient about its mean value is considered. For comparison purposes, the fluid forces are non-dimensionalized by U_n, and the normal incidence results for $Re_n = 500$ and $Re_n = 86.8$ are also reported in these plots. As mentioned in previous studies concerning rigid and flexible cylinders at lower incidence [14,39,41], a considerable amplification of the force fluctuations and mean in-line force generally occurs once the body oscillates. The magnitudes and spanwise patterns of the fluid forces clearly differ between the inclined and normal body configurations; hence, the IP is not valid. A notable feature in the inclined cylinder

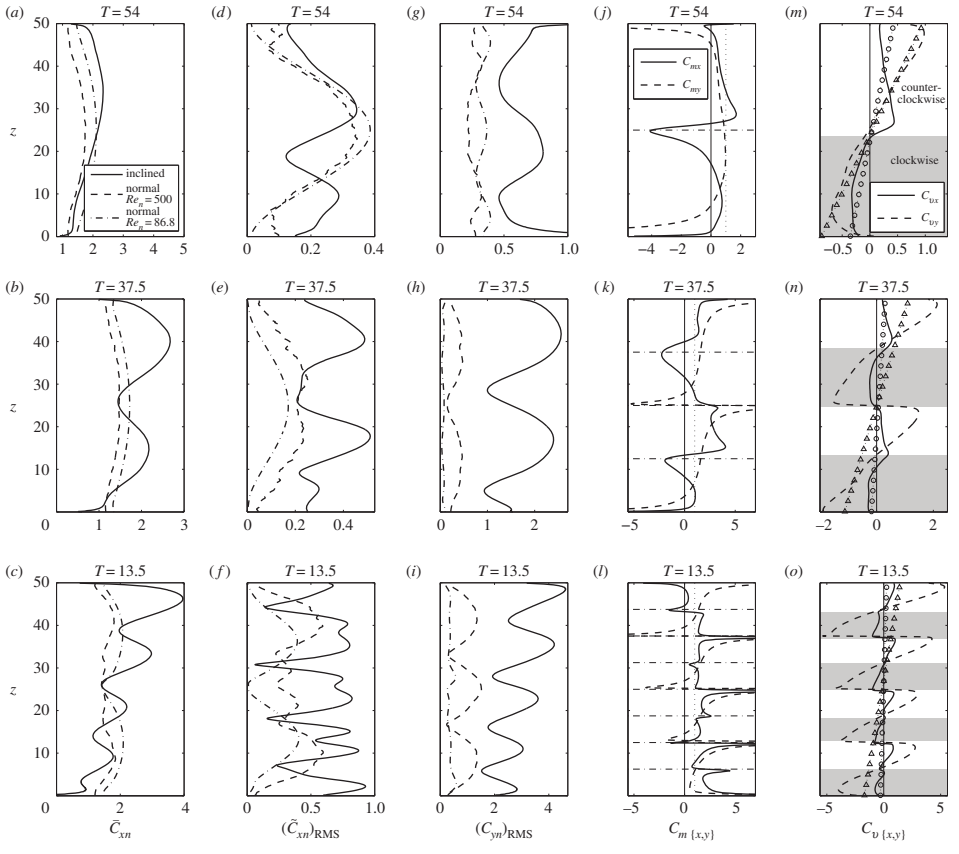

Figure 7. Spanwise evolution of the (*a–c*) mean in-line force coefficient, (*d–f*) RMS in-line force coefficient fluctuation, (*g–i*) RMS cross-flow force coefficient, (*j–l*) effective added mass coefficients, (*m–o*) mean fluid force coefficients in phase with velocity, for (*a*,*d*,*g*,*j*,*m*) $T = 54$, (*b*,*e*,*h*,*k*,*n*) $T = 37.5$ and (*c*,*f*,*i*,*l*,*o*) $T = 13.5$. Inclined and normal cylinder configuration results are reported in (*a–i*). The results in (*j–o*) concern the inclined body configuration. In (*j–l*), the potential flow value of the added mass coefficient (1) and the minima of the structural response envelope are indicated by dotted and dashed-dotted lines respectively. In (*m–o*), the white/grey areas denote the regions of the span characterized by counter-clockwise/clockwise trajectories and the linear approximations of C_{vx} and C_{vy} are represented by circles and triangles, respectively.

case is the spanwise asymmetry of the fluid forces, whereas the forces remain mainly symmetrical at normal incidence. In the inclined body case, as discussed in §4*a*, the structure in-line bending causes an asymmetry of the local inflow velocity profiles and in particular a large shear of the current locally normal to the cylinder. It appears that the mean in-line force exhibits larger magnitudes for $z > 25$, i.e. in the spanwise region associated with large values of the locally normal current velocity (figure 2*d–f*); this phenomenon is accompanied by an asymmetrical bending of the structure, as shown in figure 2*a–c*. It is recalled that additional simulations have been performed at normal incidence with a sheared current in order to match the velocity profile locally perpendicular to the inclined body; as expected, the sheared profile induces asymmetrical distributions of the forces, yet their spanwise evolutions and amplitudes still significantly depart from the inclined cylinder results.

The effective in-line and cross-flow added mass coefficients due to the fluid forces in phase with the cylinder acceleration are determined as follows:

$$C_{mx} = -\frac{2}{\pi}\frac{\overline{C_x\ddot{\xi}_x}}{\overline{\ddot{\xi}_x^2}}, \quad C_{my} = -\frac{2}{\pi}\frac{\overline{C_y\ddot{\xi}_y}}{\overline{\ddot{\xi}_y^2}}. \tag{4.4}$$

The evolutions of the effective added mass coefficients along the inclined cylinder span are plotted in figure 7*j–l*. It appears that C_{mx} and C_{my} substantially differ from the potential flow value of 1 (dotted line) and exhibit large spanwise modulations with spikes near the minima of the structural response amplitude (dashed-dotted lines). In spite of the variability of the effective added mass coefficients, it was noted in §4*a* that the actual vibration frequencies are close to the natural frequencies predicted by the dispersion relation (4.1), in which the potential flow value of the added mass coefficient is considered; such behaviour is also observed at normal incidence.

The transfer of energy between the flow and the vibrating cylinder is quantified, in each direction, through the mean fluid force coefficient in phase with the body velocity:

$$C_{vx} = \sqrt{2}\frac{\overline{C_{xn}\dot{\zeta}_x}}{\sqrt{\overline{\dot{\zeta}_x^2}}}, \quad C_{vy} = \sqrt{2}\frac{\overline{C_{yn}\dot{\zeta}_y}}{\sqrt{\overline{\dot{\zeta}_y^2}}}. \tag{4.5}$$

In the above definitions, the fluid forces are non-dimensionalized by U_{n}. Positive values of these coefficients indicate that the flow provides energy to excite the structural vibrations and negative values indicate that the body oscillations are damped by the flow. The spanwise distributions of C_{vx} and C_{vy} along the inclined cylinder are presented in figure 7*m–o*. For each value of the tension, a regular alternation of excitation and damping regions can be observed along the span and it appears that the excitation/damping zones of the in-line and cross-flow responses coincide. In the following, the spatial pattern of energy transfer is studied in relation with the spanwise evolution of the cylinder trajectory orientation. For a flexible cylinder placed at normal incidence in sheared current, the lock-in condition is preferentially established through counter-clockwise figure eight trajectories of the body; as a result, the excitation of the structure by the flow mainly occurs through this type of orbit [28,29]. In the present case of a flexible cylinder inclined in uniform current, the lock-in condition is established along the entire body length, but the energy transfer is still closely connected to the orientation of the body trajectory. To clarify this connection, the orbit orientation determined from the in-line/cross-flow response phase difference (figure 4*j–l*) is specified in figure 7*m–o*; white and grey background colours denote counter-clockwise and clockwise orbits, respectively. In all cases, it appears that the body is excited in spanwise regions where it exhibits counter-clockwise trajectories, whereas clockwise orbits are essentially associated with vibration damping. Therefore, an orientation more favourable to positive energy transfer also exists at large inclination angle. The selection of the counter-clockwise orientation for body excitation is expected to be driven by similar mechanisms to those previously described in the normal incidence case, under parallel vortex shedding (closer proximity of the cylinder and the recently shed vortices, specific phasing between body motion and vortex suction forces [16,46]). The inclined body results show that the link between energy transfer and orbit orientation persists over a range of wake configurations, i.e. parallel shedding but also oblique shedding patterns with different slant angles.

The structural responses of the inclined cylinder were all shown to exhibit a slight travelling wave behaviour, orientated towards decreasing z (§4*a*). This trend was observed under both parallel shedding and oblique shedding, where the vortex rows are moving towards increasing z; in the latter case, the structural waves and the vortices thus travel in opposite directions. This apparently paradoxical phenomenon can be elucidated in light of the spanwise pattern of energy transfer. The largest peaks of positive energy input occur for $z > 25$, and the magnitude of these peaks tends to decrease along the span. The global decreasing trend of C_{vx} and C_{vy} as z decreases is illustrated by the linear approximations of these coefficients, represented by circles and triangles in figure 7*m–o*. The space-averaged values of C_{vx} and C_{vy} are positive over the second half of the cylinder and negative over the first half; hence, the span may be separated into a global region of excitation ($z > 25$) and a global region of damping ($z < 25$). It can be noted that the region which includes the largest peaks of C_{vx} and C_{vy} corresponds to the region where the in-line bending results in the largest magnitudes of the inflow velocity locally normal to the cylinder (figure 2*d–f*) and the global direction of decreasing energy transfer coincides with the direction of decreasing magnitude of the locally normal velocity. As also reported in prior works

concerning VIV of flexible cylinders exposed to normal sheared currents [26,44], the orientation of the structural waves is determined by the energy input/output pattern: the waves follow the global direction of decreasing energy transfer, orientated from the region of large locally normal inflow velocity to the region of low locally normal velocity in the present case, and thus travel towards $z = 0$. Contrary to the inclined cylinder configuration, no monotonic orientation of the structural waves can be identified at normal incidence; this is in agreement with the absence of systematic trend of energy transfer along the span.

The analysis of the fluid forces confirms a substantial deviation from the IP at large inclination angle and emphasizes persistent features of the flow–structure system, which occur for all studied cases, i.e. regardless of the excited wavenumbers and wake configuration. In particular, a connection is established between energy transfer and some characteristics of the inclined body responses, such as the orbit orientation and the travelling wave nature of the structural vibrations.

5. Conclusion

The free vibrations of a flexible cylinder inclined at 80° within a uniform current at $Re = 500$ have been examined on the basis of direct numerical simulation results. A normal incidence configuration was also considered to assess the validity of the IP which states that the inclined and normal incidence body configurations are comparable if the normal component of the inflow velocity (U_n) is used to scale the physical quantities. The flexible cylinder was modelled as a tension-dominated structure, and three values of the tension were selected in order to cover a range of typical responses of the system. As a preliminary step, a brief overview of the fixed rigid cylinder case was presented: in the absence of body motion, the wake of the inclined cylinder is characterized by an oblique vortex shedding pattern with a large slant angle and the IP is not valid, as previously reported in the literature. The principal findings of this work can be summarized as follows.

(a) In-line and cross-flow vibrations at large inclination angle

In all studied cases, the inclined flexible cylinder is found to exhibit regular oscillations in the in-line and cross-flow directions. The structural responses consist of mixed standing–travelling wave vibrations with a predominant standing wave nature. For each value of the tension, a single frequency associated with a single structural wavenumber is excited in each direction and a ratio of 2 is observed between the in-line and cross-flow response frequencies/wavenumbers. In spite of a substantial variability of the effective added mass coefficients along the span, the vibration frequencies remain close to the structure natural frequencies. The cylinder oscillations are generally accompanied by a considerable amplification of the mean and fluctuating components of the fluid forces, compared with the stationary body case.

(b) Wake–body synchronization under parallel and oblique vortex shedding

The vibrations of the inclined flexible cylinder are excited through synchronization between the body oscillation and the vortex formation, i.e. the lock-in condition; that is why the present structural responses are referred to as VIV. It is found that, depending on the tension, the lock-in condition may involve either parallel or oblique vortex shedding patterns. In the latter case, the structural response and the wake pattern are shown to remain spatially locked, i.e. their spanwise wavenumbers coincide. In all cases, the occurrence of wake–body synchronization induces a dramatic reconfiguration of the flow pattern compared with the stationary cylinder case, with a notable reduction of the vortex shedding angle and frequency. As a general trend, the shedding angle and frequency tend to increase with the spanwise wavenumber, which increases when the tension is reduced. Regardless of the shedding angle, the wake structure resembles the 2S pattern, with the formation of two counter-rotating vortices per cycle. Owing to the frequency ratio of 2 identified between the in-line and cross-flow vibrations and to their predominant

standing wave nature, the inclined cylinder presents an alternation of clockwise and counter-clockwise figure eight orbits along its length. Wake–body synchronization occurs along the entire span, independently of the orbit orientation. However, for all the observed wake patterns, i.e. parallel shedding but also oblique shedding with different slant angles, the counter-clockwise trajectories are found to be more favourable to body excitation, whereas clockwise orbits are mainly associated with vibration damping.

(c) Deviation from the independence principle

Comparison of the vibrations and fluid forces in the inclined and normal body configurations shows that the behaviour of the system generally departs from the IP. The frequencies of the VIV occurring under oblique shedding are found to be considerably underestimated by the IP. Under parallel shedding, the response frequency of the inclined cylinder is close to the frequency identified at normal incidence, after normalization by U_n; yet, this does not imply validity of the IP, because even in this case, major differences are noted in the oscillation and force amplitudes between the two configurations. In the inclined body configuration, the flow–structure system exhibits a persistent spanwise asymmetry. Such asymmetry of the vibration and force patterns is expected because the structure in-line bending results in asymmetrical profiles of the inflow velocity components locally normal and parallel to the body; at large inclination angle, the locally perpendicular current presents a significant shear. This source of asymmetry is not captured by the IP and it appears that the response of the system remains essentially symmetrical at normal incidence. Along the inclined cylinder span, the global direction of decreasing flow–structure energy transfer is found to coincide with the direction of decreasing magnitude of the locally perpendicular velocity; this spanwise trend of energy transfer induces a monotonic orientation of the slight travelling wave behaviour of the structural vibrations, which does not exist at normal incidence.

Funding statement. The authors acknowledge support from the BP-MIT Major Projects Programme, monitored by M. Tognarelli and P. Beynet; and the Office of Naval Research under grants N00014-07-1-0135 and N00014-07-1-0446, monitored by T. Swean Jr. This work was performed using HPC resources from CALMIP (grant 2014-P1248) and GENCI (grant x20142a7184).

References

1. Blevins RD. 1990 *Flow-induced vibration*. New York, NY: Van Nostrand Reinhold.
2. Naudascher E, Rockwell D. 1994 *Flow-induced vibrations: an engineering guide*. New York, NY: Dover Publications.
3. Païdoussis MP, Price SJ, de Langre E. 2010 *Fluid-structure interactions: cross-flow-induced instabilities*. Cambridge, UK: Cambridge University Press.
4. Bishop RED, Hassan AY. 1964 The lift and drag forces on a circular cylinder oscillating in a flowing fluid. *Proc. R. Soc. Lond. A* **277**, 51–75. (doi:10.1098/rspa.1964.0005)
5. Bearman PW. 1984 Vortex shedding from oscillating bluff bodies. *Annu. Rev. Fluid Mech.* **16**, 195–222. (doi:10.1146/annurev.fl.16.010184.001211)
6. Williamson CHK. 1988 The existence of two stages in the transition to three-dimensionality of a cylinder wake. *Phys. Fluids* **31**, 3165–3168. (doi:10.1063/1.866925)
7. Mittal S, Tezduyar TE. 1992 A finite element study of incompressible flows past oscillating cylinders and aerofoils. *Int. J. Numer. Method Fluids* **15**, 1073–1118. (doi:10.1002/fld.1650150911)
8. Carberry J, Sheridan J, Rockwell D. 2001 Forces and wake modes of an oscillating cylinder. *J. Fluids Struct.* **15**, 523–532. (doi:10.1006/jfls.2000.0363)
9. Sarpkaya T. 2004 A critical review of the intrinsic nature of vortex-induced vibrations. *J. Fluids Struct.* **19**, 389–447. (doi:10.1016/j.jfluidstructs.2004.02.005)
10. Williamson CHK, Govardhan R. 2004 Vortex-induced vibrations. *Annu. Rev. Fluid Mech.* **36**, 413–455. (doi:10.1146/annurev.fluid.36.050802.122128)

11. Klamo JT, Leonard A, Roshko A. 2006 The effects of damping on the amplitude and frequency response of a freely vibrating cylinder in cross-flow. *J. Fluids Struct.* **22**, 845–856. (doi:10.1016/j.jfluidstructs.2006.04.009)
12. Benaroya H, Gabbai RD. 2008 Modelling vortex-induced fluid–structure interaction. *Proc. R. Soc. A* **366**, 1231–1274. (doi:10.1098/rsta.2007.2130)
13. Bearman PW. 2011 Circular cylinder wakes and vortex-induced vibrations. *J. Fluids Struct.* **27**, 648–658. (doi:10.1016/j.jfluidstructs.2011.03.021)
14. Jauvtis N, Williamson CHK. 2004 The effect of two degrees of freedom on vortex-induced vibration at low mass and damping. *J. Fluid Mech.* **509**, 23–62. (doi:10.1017/S0022112004008778)
15. Singh SP, Mittal S. 2005 Vortex-induced oscillations at low Reynolds numbers: hysteresis and vortex-shedding modes. *J. Fluids Struct.* **20**, 1085–1104. (doi:10.1016/j.jfluidstructs.2005.05.011)
16. Dahl JM, Hover FS, Triantafyllou MS, Oakley OH. 2010 Dual resonance in vortex-induced vibrations at subcritical and supercritical Reynolds numbers. *J. Fluid Mech.* **643**, 395–424. (doi:10.1017/S0022112009992060)
17. Trim AD, Braaten H, Lie H, Tognarelli MA. 2005 Experimental investigation of vortex-induced vibration of long marine risers. *J. Fluids Struct.* **21**, 335–361. (doi:10.1016/j.jfluidstructs.2005.07.014)
18. Chaplin JR, Bearman PW, Huera-Huarte FJ, Pattenden RJ. 2005 Laboratory measurements of vortex-induced vibrations of a vertical tension riser in a stepped current. *J. Fluids Struct.* **21**, 3–24. (doi:10.1016/j.jfluidstructs.2005.04.010)
19. Lie H, Kaasen KE. 2006 Modal analysis of measurements from a large-scale VIV model test of a riser in linearly sheared flow. *J. Fluids Struct.* **22**, 557–575. (doi:10.1016/j.jfluidstructs.2006.01.002)
20. Huera-Huarte FJ, Bearman PW. 2009 Wake structures and vortex-induced vibrations of a long flexible cylinder. I. Dynamic response. *J. Fluids Struct.* **25**, 969–990. (doi:10.1016/j.jfluidstructs.2009.03.007)
21. Modarres-Sadeghi Y, Chasparis F, Triantafyllou MS, Tognarelli M, Beynet P. 2011 Chaotic response is a generic feature of vortex-induced vibrations of flexible risers. *J. Sound Vib.* **330**, 2565–2579. (doi:10.1016/j.jsv.2010.12.007)
22. Bourguet R, Karniadakis GE, Triantafyllou MS. 2011 Vortex-induced vibrations of a long flexible cylinder in shear flow. *J. Fluid Mech.* **677**, 342–382. (doi:10.1017/jfm.2011.90)
23. Lucor D, Mukundan H, Triantafyllou MS. 2006 Riser modal identification in CFD and full-scale experiments. *J. Fluids Struct.* **22**, 905–917. (doi:10.1016/j.jfluidstructs.2006.04.006)
24. Vandiver JK, Jaiswal V, Jhingran V. 2009 Insights on vortex-induced, traveling waves on long risers. *J. Fluids Struct.* **25**, 641–653. (doi:10.1016/j.jfluidstructs.2008.11.005)
25. Bourguet R, Lucor D, Triantafyllou MS. 2012 Mono- and multi-frequency vortex-induced vibrations of a long tensioned beam in shear flow. *J. Fluids Struct.* **32**, 52–64. (doi:10.1016/j.jfluidstructs.2011.05.008)
26. Bourguet R, Karniadakis GE, Triantafyllou MS. 2013 Distributed lock-in drives broadband vortex-induced vibrations of a long flexible cylinder in shear flow. *J. Fluid Mech.* **717**, 361–375. (doi:10.1017/jfm.2012.576)
27. Bourguet R, Karniadakis GE, Triantafyllou MS. 2013 Multi-frequency vortex-induced vibrations of a long tensioned beam in linear and exponential shear flows. *J. Fluids Struct.* **41**, 33–42. (doi:10.1016/j.jfluidstructs.2012.07.007)
28. Bourguet R, Modarres-Sadeghi Y, Karniadakis GE, Triantafyllou MS. 2011 Wake-body resonance of long flexible structures is dominated by counter-clockwise orbits. *Phys. Rev. Lett.* **107**, 134502. (doi:10.1103/PhysRevLett.107.134502)
29. Bourguet R, Karniadakis GE, Triantafyllou MS. 2013 Phasing mechanisms between the in-line and cross-flow vortex-induced vibrations of a long tensioned beam in shear flow. *Comput. Struct.* **122**, 155–163. (doi:10.1016/j.compstruc.2013.01.002)
30. Van Atta CW. 1968 Experiments on vortex shedding from yawed circular cylinders. *AIAA J.* **6**, 931–933. (doi:10.2514/3.4630)
31. Ramberg SE. 1983 The effects of yaw and finite length upon the vortex wakes of stationary and vibrating circular cylinders. *J. Fluid Mech.* **128**, 81–107. (doi:10.1017/S0022112083000397)
32. Thakur A, Liu X, Marshall JS. 2004 Wake flow of single and multiple yawed cylinders. *J. Fluids Eng.* **126**, 861–870. (doi:10.1115/1.1792276)

33. Zhao M, Cheng L, Zhou T. 2009 Direct numerical simulation of three-dimensional flow past a yawed circular cylinder of infinite length. *J. Fluids Struct.* **25**, 831–847. (doi:10.1016/j.jfluidstructs.2009.02.004)
34. Zhao M, Thapa J, Cheng L, Zhou T. 2013 Three-dimensional transition of vortex shedding flow around a circular cylinder at right and oblique attacks. *Phys. Fluids* **25**, 014105. (doi:10.1063/1.4788934)
35. Willden RHJ, Guerbi M. 2010 Vortex dynamics of stationary and oscillating cylinders in yawed flow. In *IUTAM Symp. on Bluff Body Wakes and Vortex-Induced Vibrations* (*BBVIV-6*), *Capri, Italy*, pp. 47–54.
36. King S. 1977 Vortex excited oscillations of yawed circular cylinders. *J. Fluids Eng.* **99**, 495–502. (doi:10.1115/1.3448825)
37. Lucor D, Karniadakis GE. 2003 Effects of oblique inflow in vortex-induced vibrations. *Flow Turbul. Combust.* **71**, 375–389. (doi:10.1023/B:APPL.0000014929.90891.4d)
38. Franzini GR, Fujarra ALC, Meneghini JR, Korkischko I, Franciss R. 2009 Experimental investigation of vortex-induced vibration on rigid, smooth and inclined cylinders. *J. Fluids Struct.* **25**, 742–750. (doi:10.1016/j.jfluidstructs.2009.01.003)
39. Franzini GR, Gonçalves RT, Meneghini JR, Fujarra ALC. 2013 One and two degrees-of-freedom vortex-induced vibration experiments with yawed cylinders. *J. Fluids Struct.* **42**, 401–420. (doi:10.1016/j.jfluidstructs.2013.07.006)
40. Jain A, Modarres-Sadeghi Y. 2013 Vortex-induced vibrations of a flexibly-mounted inclined cylinder. *J. Fluids Struct.* **43**, 28–40. (doi:10.1016/j.jfluidstructs.2013.08.005)
41. Bourguet R, Karniadakis GE, Triantafyllou MS. In press. On the validity of the independence principle applied to the vortex-induced vibrations of a flexible cylinder inclined at 60°. *J. Fluids Struct.* (doi:10.1016/j.jfluidstructs.2014.09.005)
42. Mittal S, Sidharth GS. 2014 Steady forces on a cylinder with oblique vortex shedding. *J. Fluids Struct.* **44**, 310–315. (doi:10.1016/j.jfluidstructs.2013.11.009)
43. Karniadakis GE, Sherwin S. 1999 *Spectral/HP element methods for CFD*, 1st edn. Oxford, UK: Oxford University Press.
44. Newman DJ, Karniadakis GE. 1997 A direct numerical simulation study of flow past a freely vibrating cable. *J. Fluid Mech.* **344**, 95–136. (doi:10.1017/S002211209700582X)
45. Evangelinos C, Karniadakis GE. 1999 Dynamics and flow structures in the turbulent wake of rigid and flexible cylinders subject to vortex-induced vibrations. *J. Fluid Mech.* **400**, 91–124. (doi:10.1017/S0022112099006606)
46. Dahl JM, Hover FS, Triantafyllou MS, Dong S, Karniadakis GE. 2007 Resonant vibrations of bluff bodies cause multivortex shedding and high frequency forces. *Phys. Rev. Lett.* **99**, 144503. (doi:10.1103/PhysRevLett.99.144503)